Non-linear coupling of spiral waves in disk galaxies: a numerical study

F. Masset[1,2] **and M. Tagger**[1]

[1] DSM/DAPNIA/Service d'Astrophysique (URA 2052 associée au CNRS), CEA Saclay, F-91191 Gif-sur-Yvette, France
[2] IRAM, Avenida Divina Pastora 7, Núcleo Central, E-18012 Granada, Spain

Abstract. We present the results of two-dimensional numerical simulations of stellar galactic disks, aimed at studying the non-linear coupling between bar and spiral waves and modes, in disks with realistically peaked rotation profiles. The power spectrum analysis of the perturbed density in the disk, for azimuthal numbers ranging from $m = 0$ to $m = 4$, shows an unambiguous signature of non-linear coupling between the bar and spiral waves, or between spiral waves only, with a very sharp selection of the frequencies which optimize the coupling efficiency. It turns out that non-linear coupling can be quite efficient, and even more relevant than the Swing mechanism to account for the dynamics of the galaxy beyond the corotation of the bar. Non-linear coupling is also responsible for a number of other behaviors observed in our runs, such as harmonic or sub-harmonic excitation, and the excitation of $m = 1$ spiral waves.

Key words: galaxies: kinematics and dynamics; spiral – Galaxy: kinematics and dynamics

1. Introduction

The linear theory of spiral density waves and modes has been very successful at explaining many features of the dynamics of observed or numerically generated galactic disks. Non-linear effects (other than the generation of shocks in the gaseous component) are most often discounted, because of the small relative amplitude of the waves (i.e. the ratio of the perturbed versus unperturbed density or potential): it is usually found to be in the range 0.1–0.3, so that the quadratic terms from which non-linearities arise are of order 0.1–0.01, negligible compared to the linear ones (see e.g. Strom al. 1976).

If spiral waves could be described only by means of linear processes, each wave or mode present in the disk would

behave independently; they would be subject to the direct consequences of their linear behavior, and in particular (see Binney & Tremaine 1987, and references therein):

- they would be amplified by the Swing mechanism at their corotation radius.
- they would conserve energy and angular momentum during their propagation, except at their Lindblad resonances where they exchange them with the stars by Landau effect.
- their radial propagation can result in transient behaviors, i.e. waves emerging from the thermal noise or due to the tidal excitation of a companion, amplified once as they are reflected from their corotation radius, and traveling back to their Lindblad resonance where they are damped.
- they can also appear as exponentially growing normal modes: these result from the fact that, if a spiral wave can propagate to the galactic center, it is reflected towards its corotation radius. There it is reflected back towards the center, at the same time as it is Swing-amplified. Thus the center and corotation define a "cavity" within which the wave travels back and forth. Classically, an integral phase condition then defines a discrete set of frequencies, such that after one propagation cycle the wave returns with its initial phase; since the wave is amplified at each cycle by the same factor (say a factor Γ every cycle time τ_c), this defines an exponential growth rate $\gamma = \Gamma/\tau_c$.
- Swing amplification results from the property that waves inside corotation (i.e. inside the cavity) have negative energy, associated with the fact that their azimuthal phase velocity (pattern speed) is lower than the rotation frequency of the stars. On the other hand, as a wave is reflected inward, it excites beyond corotation a wave at the same frequency which has positive energy, because there it rotates faster than the stars, and which travels outward to the Outer Lindblad Resonance. Conservation rules then imply that the negative energy of the waves inside corotation must grow at the rate at which positive energy is emitted beyond corotation.
- in a stellar disk, spiral waves propagate only between their Lindblad resonances, where they are damped by Landau effect.

The latter effect was not a strong constraint in early numerical studies of spiral waves, which for numerical stability reasons were done in models with very weakly peaked rotation curves at the galactic center. As a consequence it was easy to find normal modes with a frequency high enough to avoid having an Inner Lindblad Resonance (ILR) near the center, yet low enough to meet their Outer Lindblad Resonance (OLR) only at a large radius, so that they could essentially extend throughout the disk. This situation changed with the introduction of faster computers, and optimized codes which allowed to deal with realistically peaked rotation profiles at the center. In that case waves can avoid crossing an ILR only if they have a high frequency, but then their OLR occurs at a rather small radius: thus any single wave or mode cannot efficiently carry energy and angular momentum over a large radial span.

In that situation Sellwood (1985), who was the first to run such realistic simulations, obtained unexpected results which were first mentioned in his study of the spiral structure of the Galaxy; the simulation showed two different $m = 2$ (i.e. two-armed) long-lived patterns, with well-defined frequencies (typical of linear normal modes) but which did not obey the usual rules associated with linear theory: the inner one, a bar, had a high enough frequency to avoid an ILR, but did not extend beyond its corotation radius located about mid-radius of the disk, implying that it should not have been amplified to reach its large amplitude. The outer pattern, on the other hand, had a lower frequency so that it did have an ILR: Landau damping should thus have forbidden it to survive for a long time in the disk.

Thus the simulation showed waves which followed in many respects the behavior expected for normal modes of the linear theory, but yet should have been forbidden by that theory; Tagger al. (1987) and Sygnet al. (1988) presented an explanation based on a remark which was later confirmed in all similar simulations: the two patterns overlapped over a very narrow radial range, which coincided both with the corotation of the inner one and the ILR of the outer one. They showed (this is in fact a generic property of non-linear wave coupling, also observed in other fields of physics, see Tagger & Pellat 1982) that this coincidence of resonances would make the non-linear interaction between the two patterns much more efficient than the crude order-of-magnitude estimate mentioned previously. A detailed kinetic description of this interaction allowed them to find that the two patterns should exchange energy and angular momentum between them and with their beat waves, namely an $m = 4$ and an $m = 0$ waves (where m is the azimuthal wave number), with respectively the sum and the difference of their frequencies. They found that these beat waves also have a Lindblad resonance at the interaction radius, and that the coincidence of these resonances does make it realistic to have a strong exchange of energy and angular momentum, i.e. a strong non-linear effect, even at relatively small amplitudes.

This made it possible to consider a scenario where the inner mode is amplified by the linear Swing mechanism, and stabilized non-linearly at a finite amplitude by transferring energy and momentum both to the outer mode and to the coupled ones, i.e. their beat waves (although the non-linear interaction could also result in non time-steady, or even chaotic, behaviors). Thus the various waves involved conspire to carry the energy and angular momentum, extracted by the first mode from the inner parts of the disk, much farther out than it alone could.

Unfortunately the absence in Sellwood's published runs of diagnostics for the $m = 4$ and $m = 0$ modes did not allow to further check this model. In a series of papers Sellwood and collaborators gave a better characterization of the behavior associated with the two $m = 2$ patterns, and presented alternative explanations. Sellwood & Sparke (1988), based on simulations by Sparke & Sellwood (1987), presented more detailed results and suggested that this behavior might be quite common in barred spiral galaxies, where it might help solve the long-standing conflict between the assumed locations of the corotations of the bar and spirals. They also pointed to an interesting feature which might make the relation with observations quite difficult: since the bar and the spiral rotate at different speeds, they should at any given time be observed at random relative azimuthal positions, i.e. with the tip of the bar and the inner tip of the spiral at the same radius, but not the same position angle (in fact Sygnet al. , 1988, noted that precisely this was suggested by Sandage (1961) for SB(r) galaxies, though Buta (1987) does not confirm this behavior). Indeed Sellwood & Sparke (1988) plot isocontours of the perturbed potential, showing this property: the bar and the spiral do form clearly detached patterns; on the other hand the isodensity contours are much more fuzzy, and hardly ever detached: this can be attributed to the fact that the density responds to the perturbed potentials in a complex manner, and manages to establish material bridges between the two patterns. This difference might explain the differing conclusions of Sandage and Buta, since observations deal mainly with the density contrast (through the complex process of star formation), and thus could not easily show the difference between the two patterns.

Sellwood & Kahn (1991) have considered an alternative explanation for the behavior observed in these simulations, based on *grooves* and *ridges* in the surface density or angular momentum distribution. They find numerically and analytically an instability, which they call the "groove mode", and which is in fact essentially the "negative-mass instability" already found by Lovelace & Hohlfeld (1978), due to either a ridge or a groove in the density profile of the disk. It is composed of waves emitted on both sides of the groove or ridge radius, and with their corotation close to that radius.

Sellwood & Lin (1989) presented a recurrent spiral instability cycle, based on this mechanism. Their simulations (made in special numerical conditions which we will discuss below) show that a transient spiral instability can extract energy and angular momentum from its corotation region, and transfer them to stars close to its Lindblad resonance. This creates a narrow feature in phase space, i.e. a groove or ridge in density space, which can give rise to a new instability with its corotation at this radius, close to the Lindblad resonance of the original wave. This new instability will in turn deposit the energy and momentum close to its Lindblad resonance, where a third one can then develop, and so on. In this manner Sellwood & Lin obtain a whole

"staircase" of spiral patterns, conspiring to carry the angular momentum outward, and such that each has its corotation close to the OLR of the previous one. They rule out mode coupling as an explanation, by interrupting the run at a given time, shuffling the particles azimuthally to erase any trace of a non-axisymmetric wave, and starting over the run. The "scrambled" simulation generates precisely the same wave as the original one, proving that in these simulations coherent coupling between the waves is not relevant.

Two main arguments make us believe that this recurrent cycle is not at the origin of the behavior discussed in what we would call the *generic* case, i.e. Sellwood's (1985) work, the present one, as well as much numerical work without the *ad hoc* numerical restrictions used by Sellwood & Lin (1989): the first argument is that in their cyclic mechanism the secondary wave is found to have its corotation at the Outer Lindblad resonance of the primary; in the generic case, on the other hand, the secondary wave is generated with its ILR at the corotation of the primary. Power density contours obtained in our simulations, as will be shown below, allow to clearly discriminate between these two possibilities, and rule out the groove mechanism as a source for the secondary in the generic case.

Furthermore, Sellwod & Lin use very artificial conditions to exhibit more clearly the physics they want to discuss, in order that it does not get blurred by all the complex, numerical or real, physics involved in a full simulation. In particular they make use of the fact that their code is written in polar coordinates to artificially eliminate any non-axisymmetric feature other than $m = 4$ – the wavenumber of the waves considered in their work. Thus non-linear coupling with the $m = 4 + 4 = 8$ is ruled out, making any comparison with the generic case dubious. Coupling with the $m = 4 - 4 = 0$, i.e. the axisymmetric component, is still possible, but then is not eliminated by the scrambling: indeed the distribution function after scrambling has every reason not to be an equilibrium one (i.e. a function only of the constants of motion, i.e. constant along epicyclic orbits) in the region of the ILR of the dominant wave before scrambling; thus $m = 0$ oscillations at the epicyclic frequency in the rotating frame, i.e. precisely at the frequency of the secondary wave found in the simulations, must be generated by the scrambling, casting at least some doubts on the exact physics of the subsequent evolution.

Thus non-linear coupling remains our preferred explanation for the behavior of "generic" simulations, and in this paper we present numerical work that substantiates this explanation. An additional incentive to do this is that in a more recent paper (Masset & Tagger, 1996b) we presented analytical work showing that non-linear coupling is a very tempting explanation for the generation of galactic warps: this is a long-standing problem, since warps (which are bending waves of the disk, very similar in their physics to spiral waves) are not linearly unstable (or extremely weakly, see Masset & Tagger 1996a); thus, contrary to spiral waves, there is no simple way to explain their nearly universal observation in edge-on galaxies, even isolated ones (see Masset & Tagger, 1996b, for a discussion of alternative explanations that have been considered). In our mechanism

the spiral, as it reaches its OLR, can transfer to a pair of warps the energy and angular momentum it has extracted from the inner parts of the galactic disk. The first warp would be the strong bending of the gaseous disk beyond the Holmberg radius, while the second one would be the short-wavelength corrugation observed within the Holmberg radius in many galaxies, including ours.

In order to study this mechanism numerically, we have written a 3-D particle-mesh code, whose results will be presented elsewhere. In a first step, we have used a 2-D version of this code for the present work, to give a more detailed analysis (which we consider as a numerical confirmation) of non-linear coupling between spiral waves and modes. Let us note that preliminary 3-D runs already give evidence of non-linear coupling between spiral waves, with an even stronger efficiency than the example presented here.

This paper is organized as follows : in a first part we present a general background about mode coupling. We present the selection rules and justify the high efficiency of coupling when the frequencies of the coupled waves are such that their resonances coincide. Since the physics of coupling can be understood without heavy mathematical derivations, we have avoided lengthy and intricate details on the derivation of the coupling efficiency, which can be found in the references given in Sygnet al. 1988, or in Masset & Tagger 1996b. In a second part we present the characteristics of the code, and in the third part we present the results of a run which shows the unambiguous signature of non-linear coupling between the bar and $m = 0$, $m = 2$ and $m = 4$ spiral waves. An additional run without the central bar is also presented in order to show that non-linear coupling is indeed responsible for the behavior observed in the external parts of the galaxy (i.e. the excitation of a slower spiral whose ILR coincides with the corotation of the bar).

2. General notions on non-linear coupling

2.1. Notations

We will note m the azimuthal wavenumber of a wave, which is an integer corresponding to the number of arms of this wave. We note ω the frequency of a wave in the galactocentric frame, with $\Omega_p = \omega/m$ the pattern frequency (in the following, including the plots, we will primarily label waves by ω rather than Ω_p).

Finally we note $\Omega(r)$ the angular rotation velocity of the stars, $\kappa(r)$ the epicyclic frequency, σ_r and σ_θ the radial and azimuthal velocity dispersion.

2.2. Non-linear coupling and selection rules

Mode coupling is a very specific non-linear mechanism (see e.g. Laval & Pellat 1972 and Davidson 1972 for a general discussion). It contrasts with the usual picture of strong turbulence, where a large number of modes interact, forming in the asymptotic limit a turbulent cascade (e.g. the Kolmogorov cascade in incompressible hydrodynamics). This asymptotic limit is reached when a whole spectrum of waves or modes is excited, with a very small correlation time, so that each mode exists only

for a very short time before it looses its energy to others (e.g. in the Kolmogorov spectrum the correlation time is of the order of the eddy turnover time). Mode coupling, on the other hand, occurs in situations where only a small number of waves or modes can exist, so that each interacts non-linearly with only a few others -ideally only two. In particular we will see in our numerical results that if the two $m = 2$ patterns interact non-linearly with an $m = 4$, the $m = 6$ that results from the coupling of one $m = 2$ with the $m = 4$ can be clearly identified, but remains so weak that its influence can be neglected (technically, since the $m = 4$ results from the non-linear interaction of two waves, it is associated with quadratic terms in the hydrodynamical equations; then the $m = 6$, resulting from the coupling of the $m = 4$ with one $m = 2$, is associated with third-order terms, which remain small). This small number of active modes translates into long correlation times, i.e. the quasi-stationary structure found in the simulations.

In a linear analysis all the waves present in the disk behave independently and do not interact. If one retains higher order terms of the hydrodynamical or kinetic equations, this is no more true and waves can exchange energy and angular momentum, provided that they fulfill a number of *selection rules*.

Let us consider two spiral density waves 1 and 2, with azimuthal wavenumbers m_1 and m_2 and frequencies in the galactocentric frame ω_1 and ω_2. The perturbed quantities relative to each wave will be of the form :

$$\xi_{1,2} \propto e^{i(\omega_{1,2}t - m_{1,2}\theta)}$$

where ξ stands for one of the perturbed quantities (a velocity component, the density or the potential). In the hydrodynamical or kinetic equations, one finds cross products of the form $\xi_1\xi_2$ and $\xi_1\xi_2^*$ (where the $*$ notes the complex conjugate), arising from non-linear terms (e.g. the $\boldsymbol{v} \cdot \boldsymbol{\nabla}\boldsymbol{v}$ or the $\rho\boldsymbol{\nabla}\Phi$ terms of the Euler equation). These terms correspond to the beat waves associated with the perturbed quantity :

$$\xi_B \propto e^{i[(\omega_1 \pm \omega_2)t - (m_1 \pm m_2)\theta]}$$

Hence the beat waves will have the frequency and wavenumber :

$$m_B = m_1 \pm m_2 \tag{1}$$

and

$$\omega_B = \omega_1 \pm \omega_2 \tag{2}$$

Thus when one performs a Fourier analysis over time and azimuthal angle of the Euler equation, at the frequency ω_B and the wavenumber m_B one will find both *linear* terms directly proportional to the amplitude of the beat wave, and *quadratic* ones proportional to the product of the amplitudes of waves 1 and 2. These terms act as a sink or source of energy for the beat wave. Two cases can then occur: the frequency and wavenumber of the beat wave may correspond to a perturbation which cannot propagate in the system; this perturbation is thus simply forced by the "parent" waves. But they may also correspond to

a wave which can propagate (i.e. they obey the linear dispersion relation); this means that the system can spontaneously oscillate at the frequency and wavenumber excited by the parents and will thus respond strongly to the excitation: just as a *resonantly driven* oscillator, the beat wave can reach a large amplitude[1]. We will see below that this is the case we study.

In that situation, since the three waves obey the linear dispersion relation and can reach large amplitudes, and since each corresponds to the beating of the other two, they can no more be distinguished as "parent" and "beat" waves: one has a system where the three waves play similar roles and can strongly interact, exchanging their energy and angular momentum. In the homogeneous (and thus much more simple) physical systems where this has been well studied, it has been found to result either in stationary behaviors (e.g. one wave is linearly unstable and extracts free energy from the system; the other two are linearly damped and can saturate the growth of the first one at a finite amplitude, by dumping the energy in a different form), or in cyclic (the classical Manley-Rowe cycles) or even chaotic behaviors (see e.g. Laval & Pellat 1972, Davidson 1972, Meunier al. 1982).

For a set of three waves such that their frequencies and azimuthal wavenumbers fulfill the relations (1-2), which are the *selection rules*, one finds linearly that the energy and angular momentum fluxes that each carry are constant; non-linearly, one finds that the time derivative of the energy density of each wave is proportional to the product of the amplitudes of the other two, i.e. these waves exchange energy and angular momentum. The derivation of the exchange rate can be done using the formalism of quadratic variational forms, and is beyond the scope of this paper devoted mainly to numerical results. The derivation of the efficiency of the non-linear coupling of bar and spiral waves is given in kinetic formalism by Tagger al. 1987 and Sygnet al. 1988, and in hydrodynamical formalism for the coupling of spiral and warp waves by Masset & Tagger, 1996b.

These papers also explain why we have not introduced in the above discussion the radial and vertical wavenumbers of the waves, which should play *a priori* the same role as the azimuthal wavenumbers or the frequencies in the selection rules. The reason is that, in theses directions, the system is inhomogeneous so that the Fourier decomposition of linear waves is irrelevant. In the vertical direction, the waves have a standing structure and one finds that the coupling coefficient is simply proportional to a scalar product of the vertical structure functions (the Fourier integrals performed in the azimuthal direction are just a particular case of this scalar product). In the radial direction, we will find that the coupling occurs over a very narrow annulus, so that the waves essentially "ignore" their radial wavelengths (which might be derived in a WKB approximation). The next section explains why we expect coupling to occur efficiently over a small

---

[1] A small point must be made about the vocabulary: because of this analogy with a resonant oscillator, this process is often called *resonant* mode coupling in the relevant litterature. Thus this term is independent of the additional factor, discussed below, that in our case the coupling occurs at a radius where the waves involved have a resonance with the particles.

radial extent. Thus, for a wave which for instance receives energy by non-linear coupling, one can consider that it is excited at that very precise radius, with a frequency and azimuthal number given by the selection rules. It will then propagate radially with a radial wavenumber given by its local dispersion relation, independent of the radial wavenumbers of the other waves.

2.3. Localization of the coupling

As mentioned in the preceding section, we can write the time derivative of the energy density of each wave as a coupling term involving the product of amplitudes of the other two. This time derivative is performed following the wave propagation, i.e. :

$$dE/dt \equiv \partial E/\partial t + (1/r)\partial(rc_gE)/\partial r = \text{Coupling Term}$$

where c_g is the group velocity, i.e. the velocity at which energy is advected radially, and the right-hand side vanishes in linear theory.

If we assume for simplicity a stationary state (we will see from our numerical simulations that this assumption is not too far from reality), we can write :

$$\partial(c_gE)/\partial r = \text{Coupling Term}$$

where we have neglected the effect of cylindrical geometry, since we expect the coupling to be very localized radially[2]. This shows in particular that wherever c_g vanishes, the variations of E can be strong even if the coupling term is not large. In fact c_g vanishes at Lindblad resonances and at the edge of the forbidden band around corotation (Toomre 1969), as can be seen from Fig. 1, so that we can expect non-linear coupling to be highly efficient when the waves are close to these radii. The physical meaning of this enhanced efficiency is simply that the waves stay in these regions for a long time, so that they can be efficiently driven, and exchange a sizable fraction of their energy, even at low energy transfer rates.

Let us note finally that if one of the waves is at its Lindblad resonance and a second one at its corotation, their beat waves, because of the selection rule on frequencies, are also at a Lindblad resonance, still improving the efficiency of non-linear coupling. This appears in a different form in the kinetic description used by Tagger al. 1987 and Sygnet al. 1988: there the coupling coefficients appear as integrals over phase space of the stellar distribution, containing two resonant denominators of the form $\omega - m\Omega$ and $\omega - m\Omega \pm \kappa$ (instead of classically only one in the linear terms leading to Landau damping), thus making the coupling efficiency very efficient when the resonances of the waves coincide.

---

[2] This assumption will be checked *a posteriori* on the numerical results in Sect. 4.3; we will see that even when the coupling partners coexist on a wide range of radii, the coupling efficiency (i.e. the energy and angular momentum exchange between these modes) is strongly peaked on a narrow annulus which will be identified as the corotation of the bar.
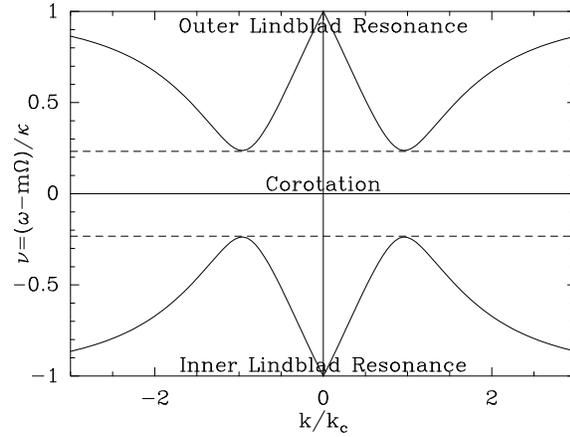

Fig. 1. This figure shows the dispersion relation of a stellar spiral density wave, in the WKB (i.e. tightly wound) approximation, for a disk with a Toomre parameter $Q = 1.05$. The critical wavevector k_c is given by : $k_c = \kappa/\sigma_r$. The quantity $\tilde{\omega} = \omega - m\Omega(r)$ is the wave frequency measured in the frame rotating with the stars. It vanishes at corotation and is equal to the epicyclic frequency at the Lindblad Resonances. The group velocity $c_g = \partial\tilde{\omega}/\partial k$ vanishes when the wave reaches the forbidden band around corotation (delimited by dotted lines) or the Lindblad Resonances, characterized by $\nu = \tilde{\omega}/\kappa = \pm 1$ and $|k/k_c| \gg 1$. Note that at small k/k_r, the wave is not tightly wound and the WKB approximation fails, so that the dispersion relation cannot be used for $|k/k_c| \ll 1$.

3. Numerical implementation

3.1. Algorithms

We have written a classical Particle-Mesh (PM) two-dimensional code simulating the stellar component of disk galaxies, with special emphasis on diagnostics adapted to the physics we describe. We have not taken into account the gaseous component, which is not expected to modify dramatically the coupling mechanism. A more detailed discussion about the role a dissipative component could play will be given in Sect. 4.4.2.

The density is tabulated on a cartesian grid using the bilinear interpolation *Cloud in Cell* (CIC). The potential is computed using a FFT algorithm with a doubling-up of the grid size in order to suppress tidal effects of aliases (see Hockney & Eastwood 1981). We use a softened gravity kernel ($\sim -G/(r^2 + \epsilon^2)^{1/2}$) for the computation of the potential, with a softening parameter ϵ chosen so as to mimic the effect of the disk thickness. Only the stars which are in the largest disk included in the grid are taken into account for the evaluation of the potential, in order not to artificially trigger $m = 4$ perturbations.

The force on each star is computed from the potential using a CIC scheme, so that the stars undergo no self-forces. The positions and velocities are advanced using a time-centered leap-frog algorithm.

Finally we have added three unresponsive static components : a central mass, a bulge and a halo. The analytical force law corresponding to each of these components is given in table 1.

Table 1. This table shows the analytical law for the central acceleration of the three static components, as well as the characteristic parameters defining each of them. The halo is not characterized by its mass which would be infinite if it extended to infinity. It is characterized instead by the asymptotic rotational velocity reached far from the galactic center.

Component	Parameters	Central acceleration
Central Mass	mass M_c	$\dfrac{GM_c}{r^2 + \epsilon^2}$
Bulge	mass M_b	$\dfrac{GM_b r}{a(b+a)^2}$
	radius b	where $a = \sqrt{b^2 + r^2}$
Halo	limit speed v_∞	$\dfrac{r_c v_\infty^2}{r^2} \mathscr{L}(r/r_c)$
	core radius r_c	$\mathscr{L}(x) = x - \tan^{-1} x$

3.2. Initialization

At the simulation startup, particles are placed at random radii with a probability law resulting in an exponential surface density profile: $\Sigma(r) = \Sigma_0 e^{-r/R_d}$, where Σ_0 is the central surface density and R_d is the length-scale of the galactic disk. All the particles have the same mass. The velocities are randomly assigned using the epicyclic approximation so that :

- The velocity distribution be a local anisotropic Maxwellian.
- The ratio of the radial to azimuthal dispersion, σ_r/σ_θ be $2\Omega/\kappa$, with Ω and κ computed consistently from the static and stellar potentials.
- The average azimuthal velocity be the rotational velocity corrected by the Jeans drift arising from the gradient of surface density.
- The Toomre Q parameter be constant over the whole disk.

Since the epicyclic approximation fails close to the galactic center, these prescriptions do not result in an exact equilibrium distribution in the central regions; we thus see in the first dynamical times of our runs relaxation oscillations, leading to a slight radial redistribution of matter in the vicinity of the galactic center.

The truncation radius of the disk corresponds to the edge of the active grid. This grid is chosen large enough so as to ensure that the runs are not perturbed by edge modes. For instance in the runs we present below the average number of particles per cell in the most external cells of the active part of the grid is $6.5 \cdot 10^{-3}$, i.e. totally negligible.

3.3. Tests

The behavior of the code has been tested so as to ensure that :

- a single massive particle follows Newton's first law, i.e. is not subject to self-force;
- two particles obey the 2-bodies laws within errors arising from finite cell size and finite timestep;

Furthermore, during a run, we check that the total angular momentum is exactly conserved (within the numerical precision errors), and that the total energy is properly conserved (within 10 %) over the whole duration of the run ; we monitor the fraction of stars ejected out of the active grid, so as to be sure that it remains sufficiently small.

3.4. Spectral analysis

The purpose of our numerical simulations is to check for the presence of non-linear coupling between waves and modes (simply defined here as quasi-stationary structures: they can thus be either linear eigenmodes, if they stay at low amplitude and unaffected by non-linear effects, or more complex non-linear entities as will be found below). We do this by identifying the features arising during the run, and checking the frequency and wavenumber relations between them.

For this we plot spectral density contours, in the same manner as Sellwood 1985: at each output time we perform a Fourier transform of the perturbed density in the azimuthal direction, resulting for each value of the azimuthal wavenumber m in spectra depending on time and radius. In order to avoid grid artifacts, we compute the spectra directly from the coordinates of each particle rather than by a Fourier Transform of the interpolated grid. Hence for each value of m, we compute :

$$W_C^{(m)}(r,t) = \sum_{i=1}^{N} \cos(m\theta_i) b(r, r_i)$$

and

$$W_S^{(m)}(r,t) = \sum_{i=1}^{N} \sin(m\theta_i) b(r, r_i)$$

where (r_i, θ_i) are the polar coordinates of the ith particle, N is the total number of particles, and, for a given r_i, $b(r, r_i)$ is a "bin"-function which linearly interpolates the value on a monodimensional radial grid.

The temporal spectrum is obtained by taking the Fourier Transform $\widetilde{W}^{(m)}(r, \omega)$ with respect to time of the complex function $W_C^{(m)}(r,t) + iW_S^{(m)}(r,t)$. We then plot either the amplitude or the power spectrum (i.e. either $|\widetilde{W}^{(m)}(r,t)|$ or $|\widetilde{W}^{(m)}(r,t)|^2$) properly normalized so as to represent either the relative perturbed density in the case of the amplitude spectrum, or the energy density in the case of the power spectrum.

Unlike Sellwood (1985), we eliminate the first timesteps when computing the temporal Fourier transform. Indeed these first timesteps correspond to a transient regime, and taking them into account degrades the spectrum and makes its interpretation more complex. The choice of the first timestep used to compute the Fourier transform is made by looking at the $W_{C,S}^{(m)}(r,t)$ plots. We start the Fourier transform when the features observed on these plots appear to have settled to the quasi-periodic behavior always obtained after a few rotation periods.

4. Results

We present two complementary runs. The first one exhibits a simple, typical example where a strong bar develops, together with a slower outer spiral; we confirm that their frequencies are such that the corotation of the bar coincides with the ILR of the spiral. The second run is performed with the same parameters, except that we inhibit the bar by changing the rotation profile at the center, so that the bar gets damped at its ILR. The rotation profile in the outer parts is not changed, and we check that the outer spiral obtained in the first run does not develop in this second one: this proves that its formation was not due to local conditions, but indeed to the non-linear excitation by the bar.

4.1. Run 1

In this run we use a 128×128-active mesh with 600 pc wide cells. The galaxy is an exponential disk of 80,000 particles with total mass $6.1 \cdot 10^{10} \ M_\odot$ and a characteristic length $R_d = 3.5$ kpc. The softening length ϵ is 300 pc. The Toomre Q parameter is initially constrained to be 1.3 over the whole disk. The disk is embedded in a static halo and a static bulge. The halo has a core radius $r_c = 2$ kpc and an asymptotic speed $v_\infty = 120$ km/s, so that the mass inside the smallest sphere containing the whole disk is 1.2 that of the disk. The bulge has a radius $b = 2$ kpc and its mass is $M_b = 5 \cdot 10^{10} \ M_\odot$. There is no central point-like mass, i.e. $M_c = 0$. We use a timestep of 0.75 Myr, we perform the simulation over 16,000 timesteps, and we output the grid density, $W_{C,S}^{(0,1,2,3,4)}(r,t)$ and some other quantities (velocity dispersion, energy, etc.) every 20 timesteps.

The chosen grid is oversized for the study of the disk, in order to avoid edge effects which have appeared to modify strongly the behavior of previous runs. Thus in all the plots and spectra we present in this paper, we have eliminated the outer parts of the active grid, where results are quite noisy due to the rarefaction of stars. In particular, all the spectra are presented on the range 0-27 kpc.

The galaxy develops a strong bar which appears a bit before 1 Gyr, and triggers a strong spiral wave outside corotation. The bar and the spiral heat the disk so that the spiral arms weaken due to the decreasing efficiency of the Swing mechanism with increasing Q. Fig. 2 shows two plots of the particle density, the first one when the bar appears, and the second one close to the end of the run, when the disk is quite hot. No striking spiral feature appears on this last plot in the outer part of the galaxy.

The simulation could be made more realistic if dissipation were included through the presence of a gaseous component, and taking into account star formation which would continuously cool the stellar population and maintain the efficiency of the Swing mechanism, so that we would still have a noticeable spiral structure even at late times. Also, since the response of the gas is strongly non-linear, we expect that it would make the outer spiral structure more prominent. But here we focus on the non-linear coupling, so that the absence of dissipation is not critical for our purpose. We will discuss later the influence it should have on the coupling.
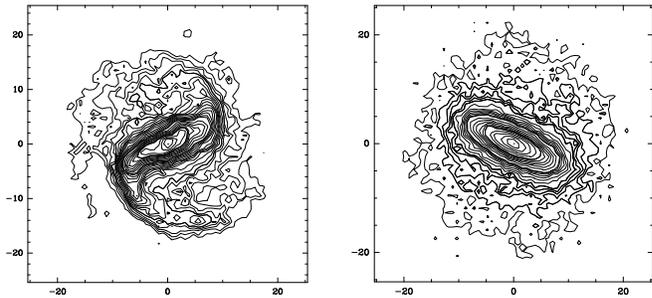

Fig. 2. The left plot is an isocontour of the grid density of run 1 at time 900 Myr. The right one represents the same quantity at time 9000 Myr. The coordinates scale is in kpc.

Let us now turn to the power spectra of the perturbed density. In Fig. 3 we have plotted isocontours of the function $W_C^{(2)}(r,t)$, i.e. the cosine contribution of $m = 2$ density perturbations as a function of radius (abscissa) and time (ordinate). This can be seen as the point of view of an observer located at radius r and $\vartheta = 0$, and seeing the bar and spiral arms sweep by with time. The lower plot represents the beginning of the simulation, from the initial time step to 2000 Myr, while the upper one shows the very end of the simulation, with time varying from 10 Gyr to 12 Gyr.

On the lower (earlier) plot we first see transient features which propagate outward, as shown by their obliquity. Between 1 Gyr and 1.5 Gyr we see the bar form, resulting in purely horizontal (i.e. standing) features. The plot clearly shows that the bar forms a quasi-stationary structure ending about 10 kpc from the galactic center, i.e. in the region of its corotation. Its corotation will slowly move outward as the bar adiabatically slows down at later times, as often seen in this type of simulations (Pfenniger & Friedli 1991, Little & Carlberg 1991). As expected from linear mode theory, the bar extends beyond corotation as a spiral wave propagating outward. The upper (later) plot shows how robust the bar is, since it has lasted for about 10 Gyr with a frequency that has slowly decreased. The right part of the diagram shows that there are still features propagating outside corotation, but that they are much less regular than the spiral waves formed from the "young" bar (in the upper part of the lower plot). This behavior which might be believed chaotic is in fact easily understood from the time Fourier Transform of this diagram (also taking into account $W_S^{(2)}(r,t)$ as imaginary part), i.e. the $m = 2$ spectral density, shown in Fig. 4. The Fourier transform is performed over 512 outputs (from 288 to 799, i.e. for time ranging from 4320 Myr to 11985 Myr).

The thinness of the features obtained shows that they correspond to quasi-stationary structures (bar or spiral) in the disk. In the inner part we see the strong contribution of the bar, which stops at corotation. Outside corotation we have two structures at different frequencies, explaining the apparent lack of periodicity in this region in Fig. 3 (there is also an intermediate, weaker structure at $\omega \simeq 22$ km/s/kpc, for which a tentative explanation will be given later). The faster wave has the same frequency as the bar and corresponds to the spiral wave excited by the bar
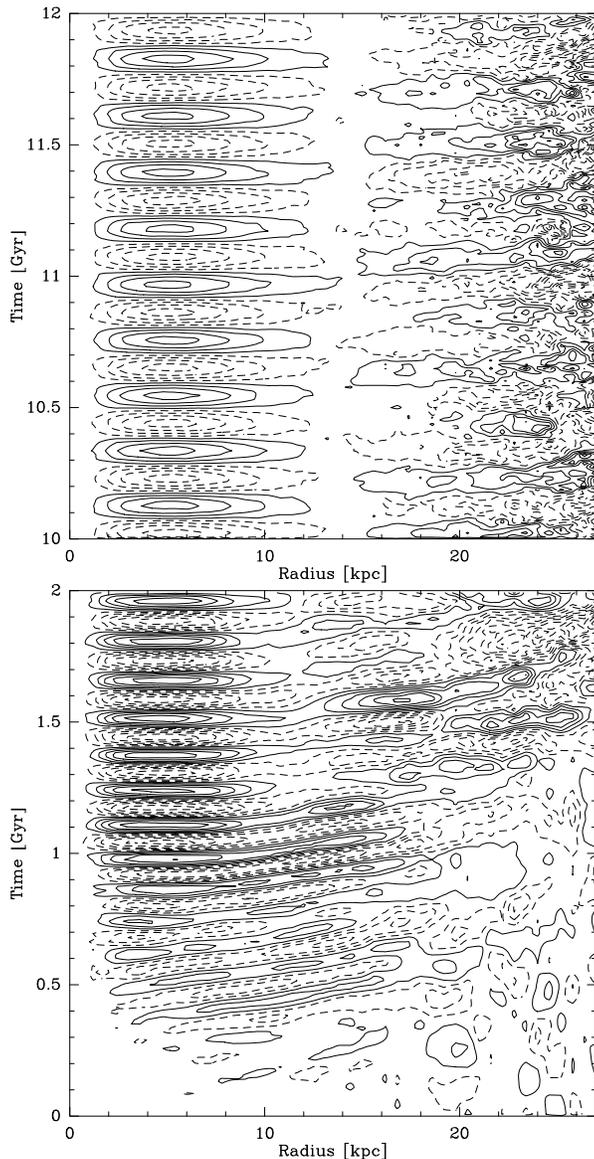
Fig. 3. The lower plot is an isocontour representation of $W_C^{(2)}(r,t)$ normalized so as to represent the relative perturbed density, with time varying between 0 and 2 Gyr. The upper plot represents the same function with time between 10 Gyr and 12 Gyr.

Fig. 4. This figure shows the $m = 2$ amplitude spectrum of the relative perturbed density. The three curves show respectively $2\Omega - \kappa$ (which gives the location of the ILR of $m = 2$ waves, depending on their frequency), 2Ω (which gives the corotation) and $2\Omega + \kappa$ (which gives the OLR) computed at time $t = 8145$ Myr, i.e. close to the middle of the time interval over which the Fourier Transform is performed. The contour spacing is 10^{-2}, and the first contour level is $4 \cdot 10^{-2}$.

through the Swing mechanism. The slower one appears to have its ILR at approximately the same radius as the corotation of the bar, as expected from the works of Tagger al. 1987 and Sygnet al. 1988. In order to check that this second mode is fed by non-linear coupling, we have to check for the presence of a beat wave near the bar corotation radius. Let us call ω_B the bar frequency and ω_S the frequency of the second (lower) spiral. We measure the frequencies from the maxima on the isocontours, with a typical accuracy ± 0.5 km/s/kpc. We find $\omega_B = 31.8$ km/s/kpc and $\omega_S = 13.9$ km/s/kpc. Hence according to equations (1) and (2) we have to check on the $m = 2 + 2$ spectrum for the presence of a mode at frequency $\omega_B + \omega_S = 45.7$ km/s/kpc, and on the $m = 2 - 2$ spectrum (i.e. an $m = 0$ mode which would ap-
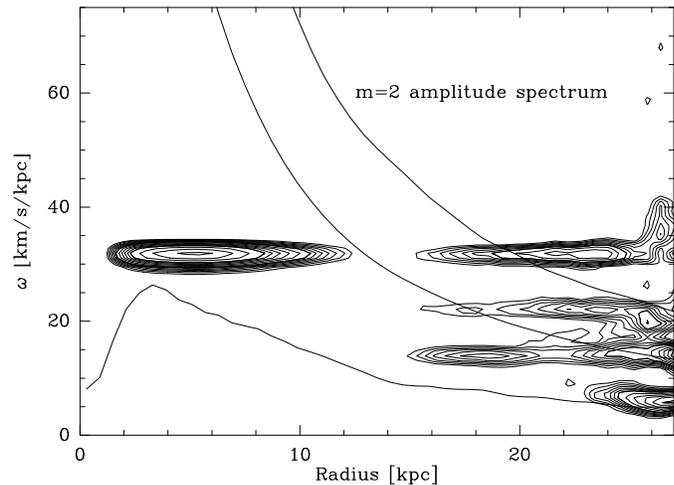
pear as a ring in the structure of the galaxy) for the presence of a mode at frequency $\omega_B - \omega_S = 17.9$ km/s/kpc. These spectra are presented respectively in Fig. 5 and 6, and the expected frequencies are indicated by a dashed line.

We have chosen to represent all the spectra of the run with the same coordinates scale. This enables the reader to check graphically for the selection rules by superimposing copies of the spectra.

On the $m = 4$ spectrum we see a major contribution corresponding to the first harmonic of the bar at $2\omega_B$, and a weaker one which is at the expected frequency, and which begins close to its ILR, i.e. also close to the expected coupling region.

Similarly on the $m = 0$ spectrum we see that a major contribution comes from the expected beat wave, which is once again located close to the corotation of the bar. More precisely, the measured frequencies are $\omega_4 = 44.7$ km/s/kpc and $\omega_0 = 18.3$ km/s/kpc, in excellent agreement with the expected ones (within 2 % for both waves).

However, the discussion above is not sufficient to ensure that the slower spiral is non-linearly excited at the bar corotation. Two questions still remain:

- Is the slower spiral really triggered by the bar, or does it exist independently of it ? The presence of $m = 0$ and $m = 4$ beat waves would still be expected in such a case, since we are dealing with finite amplitude waves, but only as "passive" features proportional to the product of the amplitudes of the parent $m = 2$ waves.
- Is the coupling localized in the bar corotation/slower spiral ILR region, as expected from the theoretical work of Tagger al. 1987 and Sygnet al. 1988 ?
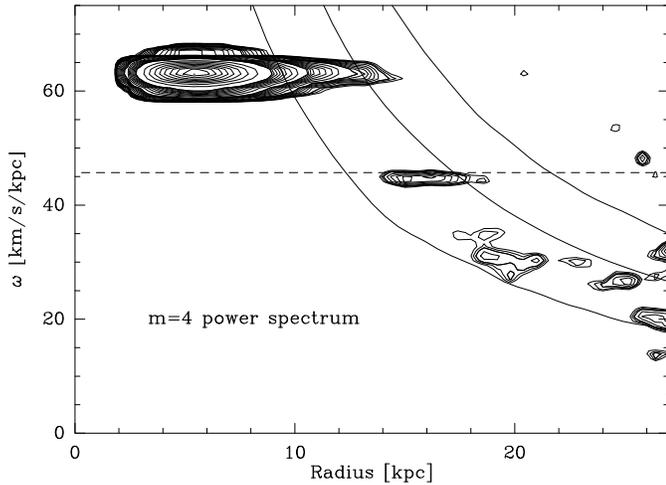
Fig. 5. This figure shows the $m = 4$ spectrum of the energy density. The three curves are respectively $4\Omega - \kappa$ (which gives the ILR of $m = 4$ waves), 4Ω (which gives the corotation) and $4\Omega + \kappa$ (which gives the OLR) computed as in Fig. 4 at time $t = 8145$ Myr. Since the radial normalization factor includes a term in $\Sigma(r)$, which has an exponential behavior, the bar is strongly enhanced and the contour levels must be adjusted in order to reveal the expected $m = 4$ beat wave. This explains the behavior of the successive isocontours in the bar harmonic at $\omega = 64$ km/s/kpc. When normalized so as to represent the amplitude of perturbed density, this $m = 4$ spectrum gives a relative perturbed density $\sigma/\Sigma \simeq 2 \cdot 10^{-2}$ for the beat wave. Taking the energy density power spectrum was necessary here to avoid strong noisy contributions on the right of diagram due to particle rarefaction at the outer edge of the disk. The dashed line indicates the expected frequency of the $m = 4$ coupling partner, i.e. $\omega_B + \omega_S$.

In order to answer the first question, we have performed a second run, almost identical to the first one, but where we have inhibited the bar formation.

4.2. Run 2

In this run we have taken a bulge mass of $M_b = 4.3 \cdot 10^{10}\ M_\odot$ and a central point-like mass of $M_c = 7 \cdot 10^9\ M_\odot$. All the other parameters are the same as in run 1. The sum of the bulge mass and the central mass equals the bulge mass in run 1, so that the rotation curve (and thus all the characteristic frequencies) coincide with the ones of run 1 at radii larger than the bulge radius. The only difference is that in this new run the ILR curve has no maximum, and thus prevents the formation of a stellar bar (or, to put it differently, the central mass is 11.4% that of the stellar disk, far above the critical value of about 5% which is thought to be sufficient to destroy the bar, (see e.g. Norman al. 1996), or even lower (2–3%, see Friedli 1994). The $m = 2$ amplitude spectrum, computed in exactly the same conditions as in run 1, is presented in Fig. 7.

Some faint standing modes (i.e. thin features) appear in this figure, but they all are far fainter than the bar and spirals of run 1 (except maybe at the outer edge where particle noise may become large). In particular one should note that the first contour
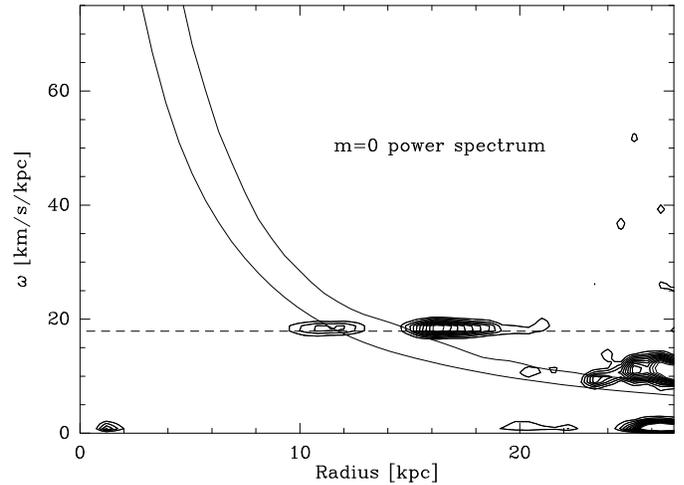

Fig. 6. This figure shows the $m = 0$ power spectrum of the relative perturbed density. The two curves are respectively Ω and κ at time $t = 8145$ Myr. Taking the energy density power spectrum was once again necessary here to avoid strong noisy contributions on the right of diagram. The dashed line indicates the expected frequency of the $m = 0$ coupling partner, i.e. $\omega_B - \omega_S$.
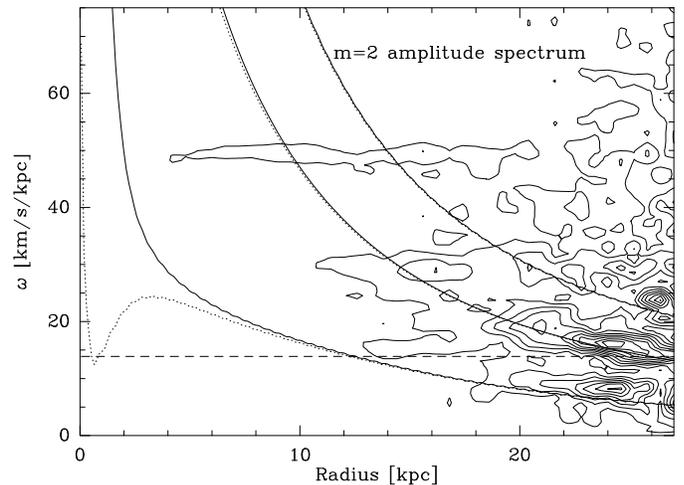

Fig. 7. In this figure we show the m=2 amplitude spectrum of run 2. The contour spacing is 10^{-2}, and the first contour is at 10^{-2}. The solid lines represent the ILR, corotation and OLR curves for run 2, and the dotted lines the same quantities for run 1. The dashed horizontal line represents the frequency at which the slower spiral was observed in run 1.

level for Fig. 4 was $4 \cdot 10^{-2}$, whereas it is 10^{-2} in Fig. 7. Obviously, in absence of the central bar, there is no standing mode in this run 2 at the frequency of the slower spiral in run 1, and the mode which appears close to this frequency is far fainter than the slow spiral in run 1.

The comparison of the stellar dispersion velocity between run 1 and run 2 is presented on Fig. 8. In the radial range where the slower spiral existed in run 1, we see that the disk temperature is the same for run 1 and run 2.
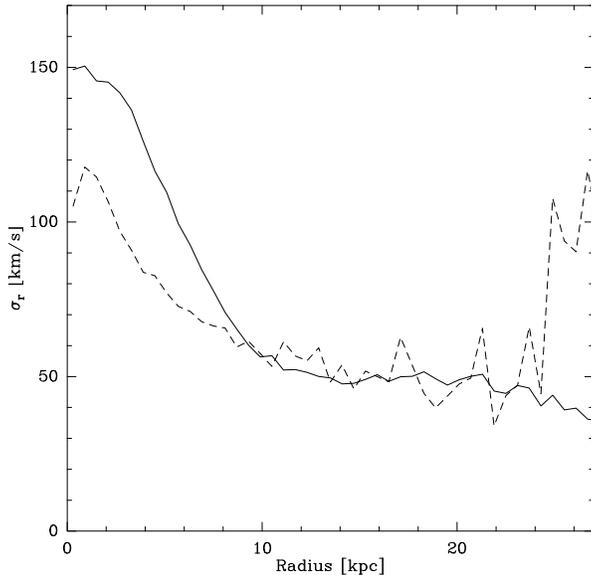
Fig. 8. Comparison of radial velocity dispersions at time 8175 Myr for run 1 (solid line) and run 2 (dashed line). The disk run 1 has been heated in its central region by the bar, but its temperature is similar to that of run 2 at radii larger than ~ 10 kpc, except for a strong peak in run 2 at the outer edge, which could not damp a wave but possibly reflect it by acting as a Q-barrier.

Hence run 1 and run 2 disk are very similar (orbital and epicyclic frequencies, temperature, density) in the region over which the slower spiral of mode 1 extended, and nevertheless no such mode appears in run 2. This is a strong point in favor of our justification of this slow spiral as non-linearly triggered by the bar.

4.3. Radial behavior of wave amplitudes in Run 1

The second question we have noted at the end of Sect. 4.1 is whether, as expected from the theoretical works, the coupling efficiency is very peaked at the bar corotation. In order to answer this question, we plot in Fig. 9 the amplitudes of the modes involved in the coupling (the slow and fast $m = 2$, the $m = 0$ and the $= 4$). The amplitudes are computed by integrating, for each value of r, the amplitude spectrum on a 1.6 km/s/kpc bandwidth centered on the peak frequency of the mode.

In this figure we clearly see from the solid line that, in agreement with linear theory, the separation between the bar and the Swing triggered spiral occurs at 13 kpc, i.e. almost exactly where the corotation appears to be located according to Fig. 4.

For $r > 13$ kpc the Swing-triggered spiral and the slower, non-linearly excited one grow very similarly up to 18 kpc. One can note that the amplitudes of the $m = 0$ and $m = 4$ waves are clearly not proportional to the product of the amplitudes of the fast and slow $m = 2$ spirals: in that case (where these waves could be simply understood as ordinary beat waves, rather than partners in a non-linear mechanism), the $m = 0$ and $m = 4$ curves would peak around 18 kpc, and they would have a
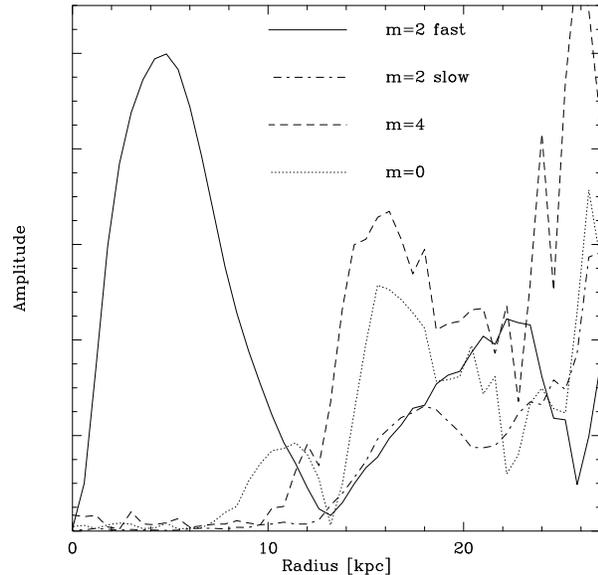

Fig. 9. The relative amplitudes of the modes, computed as explained in the text. The ordinates scale is arbitrary, but is the same for both $m = 2$ on one hand, and for $m = 4$ and $m = 0$ on the other hand.

parabolic shape between 13 and 18 kpc, since both $m = 2$ curves are linear on this range. Instead of this behavior, both curves raise sharply around 14 kpc and peak around 16 kpc. This is a strong indication that the coupling is very localized; indeed, just as the slow $m = 2$, the $m = 0$ and $m = 4$ are generated at this coupling radius, and then propagate freely in the disk. Hence the coupling partners can coexist on a wide range of radii whereas the non-linear coupling mechanism which makes them interchange energy and angular momentum takes place at a very well defined radius.

Around 18-19 kpc, the $m = 4$ is attenuated. This is reasonable since it reaches there its corotation, and thus the "forbidden band" where it does not propagate (just as the fast $m = 2$ at 14 kpc); on the other hand the $m = 0$ is also attenuated, something we could not expect from its linear properties. This can be understood by returning to the energy spectrum of the $m = 4$, Fig. 5: one sees, at 30 km/s/kpc, another quite strong $m = 4$ feature with its ILR at the corotation of the previous one; this is quite close to the 26 km/s/kpc, expected for the beat wave of the previous $m = 4$ and of the $m = 0$; we believe that non-linear coupling is at work also here, allowing the $m = 0$ and the fast $m = 4$ to transfer their energy to a slower one. This would be an illustration of the "staircase" of modes often observed in these simulations.

Finally, one could wonder why the fast $m = 2$ seems to extend (and even to be peaked) beyond its OLR. Actually this behavior disappears if we consider the energy density rather than the amplitude, as depicted on Fig. 10.

In this figure we see that the fast $m = 2$ spiral peaks around 20 kpc, where its OLR is expected. There is still a noticeable energy density up to 2 kpc farther. This is in agreement with the epicyclic radius (which is the natural width of the resonance)
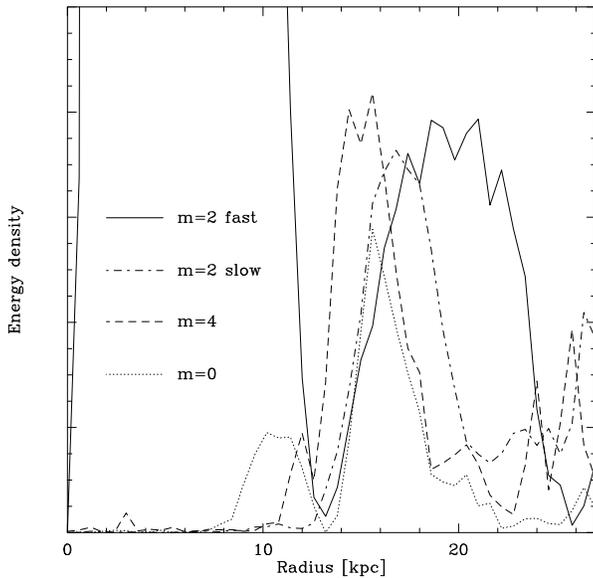
Fig. 10. This figure shows the mode energy density, computed in a similar way as the amplitude at the previous figure (in particular over the same bandwidth). Once again the vertical scale is arbitrary, but is the same for both $m = 2$ and for both $m = 0$ and $m = 4$.

of about $\sigma_r/\kappa \sim 3$ kpc. One can note once again on this plot that the $m = 4$ extends only to its corotation at $r \simeq 18$ kpc, and that the $m = 0$ also ends in this region, while the slow $m = 2$ extends to ~ 21 kpc.

4.4. Varying parameters in Run 1

In order to check the influence of the parameters of run 1 on the spectra and on the disk profile temperature (which might be strongly influenced by two-body relaxation in a 2D simulation), we have repeated run 1 with twice as many particles, or with the same number of particles but with a timestep of 0.25 Myr, three times smaller than the initial one.

When we perform run 1 with a double number of particles, the same features remain, i.e. the bar, the Swing triggered spiral and the slower spiral, at frequencies which have varied by no more than 1 km/s/kpc. The coupling partners also remain, with the same intensities. As expected, the outer part of the spectra is less noisy since the particle noise has decreased. Furthermore, the intermediate faint $m = 2$ standing mode of figure 4 at 22 km/s/kpc almost disappears. This is understandable since a good explanation for this mode is the subharmonic excitation of the $m = 4$ coupling partner, and subharmonic excitation requires initial noise to start. Since the noise is decreased in this new run, the corresponding mode is accordingly fainter. The same kind of argument stands for the alternative mechanism one could consider to justify this mode, which is the groove or ridge mechanism of Sellwood & Lin 1989. Whatever the correct explanation for this mode may be, the non-linear coupling mechanism which excites a slower spiral at its ILR and at the

bar corotation is far more relevant to account for the dynamics of the external part of the galaxy.

Let us mention that with twice as many particles, the temperature profile obtained in the disk coincides with the one observed with the initial number of particles (i.e. $80,000$). This shows that the heating in the simulations is due to the presence and growth of the spiral and the bar, and not to two-body relaxation.

When we perform run 1 with a smaller timestep (0.25 Myr instead of 0.75 Myr), we obtain the same results (i.e. the same features on all the spectra, with frequencies that have varied by no more than 0.5 km/s/kpc), showing that the timestep chosen for run 1 was sufficiently small.

4.5. Discussion about Run 1

4.5.1. Non-linear coupling versus grooves

Run 1 confirms the coincidence of the corotation of the inner (fast) mode and the ILR of the outer (slow) one, as noticed in the simulations of Sellwood 1985 by Tagger al. 1987 and Sygnet al. 1988. This differs from the mechanism of Sellwood & Lin 1989, from which one would expect to have the corotation of the outer mode at the OLR of the inner one: Fig. 4 allows to clearly rule out this mechanism here, since the OLR of the fast mode is at about 20 kpc, whereas the corotation of the slow one is at about 25 kpc. The run also confirms the presence of coupled $m = 0$ and $m = 4$ waves at significant amplitudes.

Since the slower spiral is long-lived (as shown by the thinness of the isocontours in Fig. 4) although it has an ILR where it should be damped, it must be continuously fed. We attribute this, following the analysis of Tagger al. 1987 and Sygnet al. 1988, to non-linear coupling between the two $m = 2$ modes and the $m = 0$ and $m = 4$ beat waves.

We also wish to mention the intermediate faint spiral mode at $\omega = 22$ km/s/kpc, observed in Fig. 4, whose corotation roughly coincides with the OLR of the fast spiral. This mode could then correspond to a groove or ridge excited mode, following the mechanism of Sellwood & Lin 1989. However the energy flux it carries is far lower than the one transported by the fast and slow spirals. The excitation of this mode, which appears nearly halfway in frequency between the fast and slow spirals, could have other explanations:

- it could correspond to the subharmonic of the $m = 4$ beat wave, since it has half its wavenumber and nearly half its frequency. It would be excited at its corotation where both waves are resonant.
- its OLR coincides with the corotation of the slow spiral, so that it could be non-linearly fed by this slow wave. In favor of this explanation, one can notice that the low frequency, outer feature observed on the $m = 0$ power spectrum (slightly below 10 km/s/kpc) would be an obvious partner in this coupling.

A combination of these three mechanisms is probably at work in the generation of this intermediate $m = 2$ feature, and much more detailed simulations, with some additional theoretical work, would be needed to understand their interplay. This
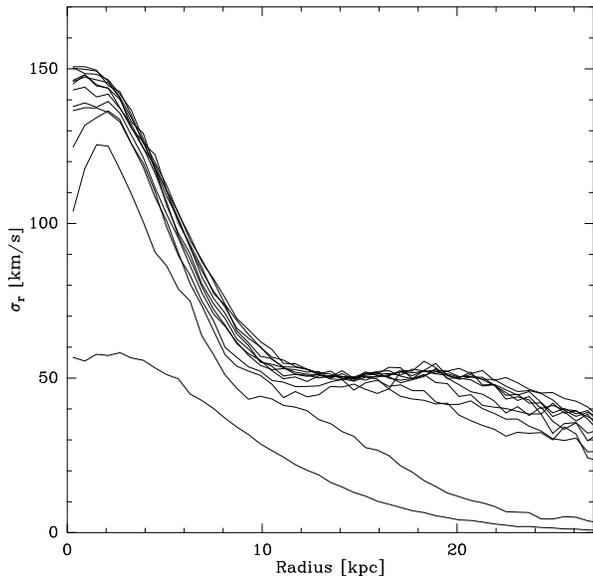
Fig. 11. This figure shows the radial velocity dispersion as a function of radius for times 0, 1, 2...11 Gyr. The lowest curve is for $t = 0$, the intermediate one is for $t = 100$ Myr and the other ones almost coincide. Since $Q \equiv 1.3$ at all radii initially, one sees that, for $t > 100$ Myr and $r \sim 15$ kpc, Q is far above one, strongly limiting the efficiency of non-linear coupling.

might be taken as an illustration of the fact that, at lower amplitudes than the dominant features we have analyzed, one enters in the regime of multiple non-linear interactions between numerous partners, which could lead in other conditions to a turbulent cascade, as discussed in the introduction.

4.5.2. Comparison of Swing and non-linear coupling

An important difference between run 1 and the simulation of Sellwood 1985 (and many of our own runs) is that in the latter case the fast mode did not extend beyond its corotation, whereas here the Swing-triggered spiral (at the frequency of the bar) is nearly as strong as the slower one up to 18 kpc, which corresponds to the corotation of the $m = 4$ coupled wave, and then even dominates it. The reason is that for this first run, in order to simplify the physics involved, we have chosen parameters which optimize the initial efficiency of the Swing, resulting in a very strong bar. Also, since Sellwood's work clearly documents a case where the bar does not extend beyond corotation, we have chosen this run here so as to show that both behaviors are possible.

We also note, in reference to run 1, that the coupling efficiency, which increases when the group velocities decrease as explained in Sect. 2.3, is expected to vary as $\sigma_r^{-3/2}$, where σ_r is the radial velocity dispersion (see Masset & Tagger, 1996). Since a realistic disk (i.e. with a dissipative component) would remain much colder than the disk of run 1, we expect non-linear coupling to be far more efficient in a realistic disk. Fig. 11 shows how the disk has been heated by the bar.

We see that around the corotation of the bar, where coupling occurs, the Toomre Q parameter reaches values of 4 to 5 as soon as the bar forms. For a colder disk, with $Q \sim 1.5$, non-linear coupling could be up to 6 times more efficient.

On the other hand, the Swing mechanism also becomes less efficient as Q increases. Thus a realistic simulation including a gaseous component and stars formation would be necessary to check how the energetics of the Swing-triggered spiral and that of the slower one compare in a realistic barred galaxy, as a function of local or global parameters of the disk.

5. Conclusion

We have presented a typical numerical simulation of a barred spiral galaxy, which shows a strong and unambiguous signature of non-linear coupling between bar and spiral waves. This non-linear coupling is responsible for the excitation by the central bar of a slower, outer $m = 2$ spiral wave which can efficiently carry away the energy and angular momentum extracted from the central regions by the bar. This confirms, with more detailed diagnostics, the simulations of Sellwood 1985 and the theoretical explanation of Tagger al. 1987, and Sygnet al. 1988.

This behavior is in fact routinely observed in numerical simulations, as soon as one introduces realistically peaked rotation profiles at the center, so that Lindblad resonances prevent any single spiral mode to extend radially over most of the galactic disk. This leads us to believe that non-linear coupling can be frequent also in real galaxies, under different forms, which may be difficult to analyze because of the complex density patterns (Sellwood & Sparke 1988), as discussed in the introduction:

- As mentioned by Sygnet al. 1988, and in our introduction, SB(r) galaxies seem to be a very good candidate, because of the mismatch between the position angles of the bar and spiral found by Sandage (1961). The disagreement of Buta (1987) on this observation might be attributed to the above-mentioned complex density patterns, so that this clearly deserves further investigations.

- As discussed by Sellwood & Sparke 1988, this mechanism might help solve the long-standing difficulties found when one tries to locate the corotation in many barred spirals.

- Recent work based both on observations and more complex simulations (Friedli & Martinet, 1993; Friedli al. , 1996) has pointed to the frequent observation of "bars within bars" in the central regions of galaxies. They have shown that the inner bar is most frequently misaligned with the outer one, ruling out a purely dynamical origin (such as stars aligned on x_2 orbits, perpendicular to the main bar). Non-linear coupling, shown here to occur at larger radii, appears as a very good tentative explanation for this mechanism, which should play a major role in the fueling of the inner parts of the galaxy.

- M 51 might provide a clue to the same mechanism in tidally-driven spirals. Elmegreen al. (1987), in detailed modeling of the spiral structure in three "classical" galaxies, found that the structure of M 51 could be explained only by the presence of two distinct spirals, and noticed (before they knew about our work) that the corotation of the inner one

would coincide with the ILR of the outer one – the signature of our mechanism. One must naturally be cautious with this result, since the modeling of M 51 has proven to be a very challenging task. However, precisely because there remains much to be done in this respect, and because new observations become available, we believe that this might very well prove to be an important element in the complex physics of M 51.

– There has been in recent years a renewed interest in $m = 1$ spiral structures. The linear theory of the $m = 1$ mode in galaxies, which differs markedly from $m > 1$ ones, remains to be done, but it is generally believed that it is not or only weakly unstable. Work done in the context of accretion disks (Adams al. , 1989) would not really apply here, because self-gravity is strong and the boundary conditions used are different (see also Noh al. , 1991). Tagger & Athanassoula (1990) discussed non-linear coupling of an $m = 2$ with two $m = 1$ modes, as a possible explanation for the structure of lopsided galaxies. They appear as the strong version of a more frequent observation, that of off-centered nuclei (i.e. nuclei affected by an $m = 1$ displacement) in galaxies - including our own. Miller & Smith (1992) for stellar disks, and Laughlin & Korchagin (1996) for gaseous ones, have found persistent such motions in numerical simulations, a behavior we also obtain: although our cartesian grid gives insufficient resolution at the center to give it strong confidence without additional work, we do find $m = 1$ spirals at the center, non-linearly coupled to unstable $m = 2$ and $m = 3$ ones.

– As mentioned in the introduction, we (Masset & Tagger, 1996b) have shown from analytical work that non-linear coupling with spiral waves is also a very tempting explanation for the generation of warps in disk galaxies. Work is in progress to give numerical evidence of this mechanism.

References

Adams, F.C., Ruden, S.P., and Shu, F.H., 1989, ApJ, 347,959
Binney, J., and Tremaine, S., 1987, Galactic Dynamics, Princeton University Press, J.P. Ostriker ed., pp. 376 et sq.
Buta, R., 1987, ApJS, 64, 383
Davidson, R.C., 1972, Methods in Nonlinear Plasma Theory, Academic Press, New-York
Elmegreen, B.G., Seiden, P.E., and Elmegreen, D.M., 1989, ApJ 343, 602
Friedli, D., 1994, in: Mass-Transfer Induced Activity in Galaxies, ed. I. Shlosman. Cambridge University Press, Cambridge, p. 268
Friedli, D., Martinet, L., 1993, A&A 277, 27
Friedli, D., Wozniak, H., Rieke, M., Martinet, L. and Bratschi, P., 1996, A&AS 118, 461
Hockney, R.W., and Eastwood, J.W., 1981, Computer Simulation Using Particles, McGraw-Hill, New York
Laughlin, G., and Korchagin, V., 1996, ApJ 460, 855
Laval, G., and Pellat, R., 1972, in: Cours des Houches 1972, Eds. De Witt, C. and Peyraud, J., Gordon and Breach, 1975
Little, B., and Carlberg, R.G., 1991, MNRAS 250, 261
Lovelace, R.V.E., and Holhfeld, R.G., 1978, ApJ 221, L51
Masset, F., and Tagger, M., 1996a, A&A 307, 21
Masset, F., and Tagger, M., 1996b, to appear in A&A
Meunier, C., Bussac, M.N., and Laval, G., 1982, Physica 4D p. 236
Miller, R. H. and Smith, B. F, 1992, ApJ 393, 508
Noh, H., Vishniac, E.T., and Cochran, W.D., 1991, ApJ 383, 372
Pfenniger, D., and Friedli, D., 1991, A&A 252, 75
Sandage, A., 1961 *The Hubble Atlas of Galaxies*, Carnegie Institute, New York
Norman C.A., Sellwood J.A., and Hasan, H., 1996, ApJ 462, 114
Sellwood, J.A., 1985, MNRAS 217, 127
Sellwood, J.A., and Sparke, L.S.,1988, MNRAS 231, 25p
Sellwood, J.A., and Lin, D.N.C., 1989, MNRAS 240, 991
Sellwood, J.A., and Kahn, F.D., 1991, MNRAS 250, 278
Sparke, L.S., and Sellwood, J.A., 1987, MNRAS 225, 653
Strom, S.E, Jensen, E.B., and Strom, K.M., 1976, ApJ 206, L11
Sygnet, J.F., Tagger, M., Athanassoula, E., and Pellat, R., 1988, MN-RAS 232, 733
Tagger, M. and Pellat, R., 1982, Plasma Phys. 24, 753
Tagger, M., and Athanassoula, E., 1990, in IAU Coll. 146, F. Combes and F. Casoli eds., 105
Tagger, M., Sygnet, J.F., Athanassoula, E., and Pellat, R., 1987, ApJ 318, L43
Toomre, A., 1969, ApJ 158, 899